Everest Advances in Science and Technology (EAST) Vol. 2, No. 1, 2026 (Special Issue)
ISSN: 3102-0410 (Print), 3102-0429 (Online)
DOI: https://doi.org/10.3126/east.v2i2.99473

Research and Development of Geosynthetic Applications for Flexible Pavement Systems: Numerical Modeling, Data Validation, and Design Catalog

AANCHAL TIWARI[1], RAM C. TIWARI[1], PRABHAT K. JHA[2], DHANAPATI DHAKAL[3], BIJAYA BHUSAL[3], KABIN LAMICHHANE[3], BIJAYA BHATTARAI[3], DIWAS K. CHHETRI[3], AND AAYAM TIWARI[4*]

Abstract. This research offers an extensive analysis of the usage of geosynthetics, specifically geotextiles and geogrids, in flexible pavement systems as a design catalog. The research utilizes numerical modeling that is confirmed using DOR sheet and IIT-Pave. Field validation will also be carried out. Numerical modeling was carried out using advanced Finite Element Method (FEM) simulations with PLAXIS 3D to determine the impact of geogrid-reinforced pavements under static and dynamic axle loading. The findings reveal considerable decrease in vertical compressive strains at the subgrade layer and horizontal tensile strains at the top of the base layer indicating better load distribution and improved structural performance. The presence of geogrid improves the pavement performance through reduction of deformation and strain in important layers with performance dependent upon pavement thickness, stiffness of geogrid and its position in the base. Placement of geogrid at the subbase-subgrade interface leads to considerable reduction in vertical strain (3.61%-19.52%) and horizontal strain at asphalt-base interface in range of 18.72% to 41.08%. Reduction in thickness of pavement in range of 15 mm to 170 mm for traffic loading of 5 to 30 Million Standard Axles (MSA) and subgrade CBR value in range of 5% to 12%. Validation through field tests using strain gauges and earth pressure sensors under vehicle load (Tipper and Ford trucks) supports the numerical findings. The research offers material specifications and design catalog in the form of handbook, enabling cost-effective and sustainable pavement solutions.

Keywords: Finite Element Method (FEM), Flexible Pavement, Geogrid Reinforcement, Pavement Design, Design Catalog

[1] Pulchowk Campus, Institute of Engineering, Tribhuvan University, Lalitpur, Nepal

[2] Ministry of Physical Infrastructure and Transport (MoPIT), Government of Nepal

[3] Thapathali Campus, Tribhuvan University, Kathmandu, Nepal

[4] Advanced College of Engineering and Management, Kathmandu, Nepal

Email: aayam2003@gmail.com

[*] Corresponding author

Manuscript received: 24 March 2026; Revised: 15 June 2026; Accepted: 11 July 2026.

1. INTRODUCTION

The inevitable shortcomings of traditional M-E design techniques-in particular, their use of linearized multilayer elasticity theory-are inadequate in modeling the nonlinear constitutive behavior and the SSI effect in reinforced pavement structures. The proposed study is aimed at solving these problems through the utilization of three-dimensional FEA using Plaxis 3D software that offers a powerful computer-based tool for investigating the sophisticated interaction and lateral confinement characteristics of geosynthetics. Using site-specific geotechnical properties of Pulchowk Campus area, the research confirms the applicability of the sophisticated numerical model that allows predicting the accurate mechanical behavior of the flexible pavement subjected to various loading scenarios [1, 2].

From the point of view of numerical simulations, it has been established that the effectiveness of the pavement structure depends significantly on the location of the reinforcement layer. It has been proven experimentally that the geogrid placement at the interface between the subbase and the subgrade produces the optimal reduction of the vertical strains at the top of the subgrade layer. The optimized tensioning membrane effect and the lateral confinement of the base aggregate provide for a better load capacity of the pavement and the even distribution of the vertical stresses in the underlying layers [3, 4].

Finally, the incorporation of geogrids results in the significant reduction of the permanent deformations. The control of the stress-strain behavior under cyclic loads helps prevent the fatigue cracking and the subgrade rutting-a key problem in the extended life span of road infrastructures [5, 6].

1.1. **Structural Optimization and Design Standardization.** Beyond performance enhancement, this study proves that there exists an opportunity for considerable thickness reduction in structural layers of the pavement. Based on the FEA results, it is found that geogrid-reinforced pavement sections may achieve equal or better structural numbers with lower thickness of the base layer as compared to unreinforced pavement structures. This optimization provides a reasonable way of achieving material conservation and cost savings during the design process without any decrease of reliability and performance of the system [7, 8].

These results are summarized in the form of a special design catalogue of geogrid-reinforced flexible pavements which gives the technical basis for material choice and placement strategies [9]. A comparative analysis of the performance of this design approach versus the Flexible Pavement Design Guide (2021) proves that the conventional unreinforced approach is rather conservative. It is shown that geogrid-reinforced pavements always have higher stress resistance and efficiency of structural coefficient than the conventional designs; therefore, there is a need to revise the contemporary design standard to include geosynthetic solution [10, 11, 12, 13].

Although the current models are adjusted to specific lithology and climate of the Pulchowk Campus area, they offer the methodology for precise design of the flexible pavement structures; however, additional research is needed for the development of the rigid and composite pavement designs.

2. METHODOLOGY

The engineering properties of the subgrade soil are listed in Table I showing the CBR test results at different dry densities for (a) Soil S1 and (b) Soil S2 by carrying out compaction at different efforts.

Direct shear tests indicated that Sample S1 had a cohesion of 45.4 kg/cm^2 and an internal friction angle of 12.84°, while Sample S2 showed a cohesion of 34.89 kg/cm^2 and a higher friction angle of

Table 1. CBR in different dry density maintained with varying blows: (a) of Soil S1 and (b) of Soil S2

	Dry density (gm/cc)	CBR
S1	2.01	13.33
	1.91	12.86
	2.04	14.29
	1.74	11.17
S2	1.70	9.71
	1.78	17.38
	1.72	13.81
	1.68	8.97

25.40°.

2.1. **Design of Reinforced Flexible Pavement.** Pavement design was then performed in accordance with the Flexible Pavement Design Guidelines [14] utilizing soaked CBR values and design traffic loading of 20 million standard axles (msa). Three types of pavement were designed to evaluate their performance: (1) the pavement without reinforcement design; (2) the pavement with reinforcement of the same thickness as the previous one to evaluate the effect of geogrid reinforcement on the performance; and (3) the pavement with reinforced but thinner layer optimized by numerical modeling.

2.2. **Standard Axle Load Configuration.** Loading details are taken from IRC 37:2018 [15] and its graphical representation are present in Figure 1.

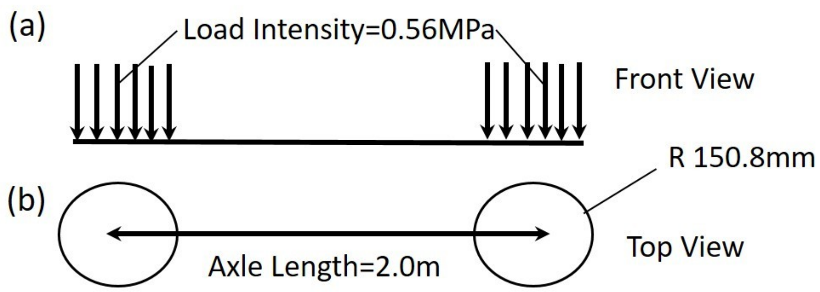

Figure 1. Wheel load configuration: (a) front view showing loading intensity of tyre and (b) top view showing contact area dimension.

2.3. **Properties of Geogrid.** Axial stiffness is the ratio between the force per unit width in the axial direction and axial strain (elongation divided by original length). For isotropic material, shear stiffness is equal to half of the axial stiffness ($G_A = E_A/2$), according to Plaxis 3D manual.

A biaxial geogrid with stiffness of 700 kN/m at 2% strain has been selected using laboratory data for geosynthetics. This geogrid has been modeled as elastic material. The properties of the geogrid have been obtained from the manufacturer specifications given in Table II.

TABLE 2. Geogrid Strength Properties

Testing method	EN ISO 10319 ASTM D 6637
Geogrid type	40S
Tensile strength at 2% strain Longitudinal	14 kN/m
Tensile strength at 2% strain Transverse	14 kN/m
Stiffness calculated (longitudinal)	700 kN/m
Stiffness calculated (transverse)	700 kN/m

2.4. **Finite Element Modelling.** The numerical model will be designed in PLAXIS 3D, where both geometry and layer parameters will be the same as those in the physical model. Linear elastic material behavior will be considered for the subgrade, granular layer, and surface layer, whereas the geogrid will be modeled as a surface element. The load will be applied in the form of two point loads of 40 kN at an axle distance of 2 m.

2.5. **Model Geometry.** The study considers an area of a two-lane highway, whereby the carriageway has a width of 3.5 m per lane and shoulders on both sides measuring 0.75 m each, resulting in a total pavement width of 8.5 m. The length of the model has been considered as 10 m. The thicknesses of various layers, such as base, subbase, DBM, and AC, have been considered according to the DoR (2014) guidelines for designing flexible pavement.
Although the subgrade layer theoretically extends to infinity, a thickness of 3 m has been considered in the present model. This depth has been selected based on the pressure bulb theory of Boussinesq, as only 5.3% of the surface stress reaches this depth.

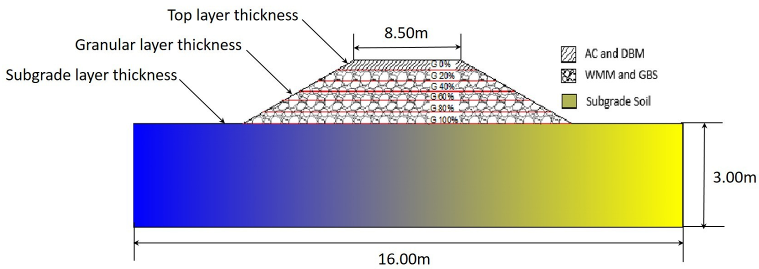

FIGURE 2. Detailing of model.

2.6. **Finite Element Analysis.** Finite element analysis requires an iterative process of calculations to determine stresses and strains, and the results converge within specified boundary conditions. Therefore, proper selection of boundary conditions is crucial for realistic representation of field conditions, ensuring that displacement near the model boundaries remains consistent with actual site conditions.
This study uses "normally fixed" boundary conditions, in which vertical boundaries are fixed normal to their planes and free in other directions. However, "fully fixed" boundary conditions restrict movement in all directions, while "free" boundaries allow movement in all three directions. Moreover, "viscous" boundaries absorb outgoing wave energy, whereas "none" boundary applies default fixity conditions.

2.7. **Optimum Position of Geogrid on Pavement.** After preliminary evaluation of geogrid efficiency, a comprehensive numerical analysis was carried out to determine the optimum location of the geogrid within the granular material layer. Geogrids were placed at five different positions in the pavement structure, namely 0%, 20%, 60%, 80%, and 100% of the total base thickness (WMM+GSB), to evaluate their effect on stress distribution and deformation behavior.
This analysis enabled comparison of reinforcement efficiency at different locations within the pavement structure.

Simulation analysis was carried out for biaxial geogrids with stiffness of 700 kN/m under a traffic load of 10 msa for subgrade CBR ranging from 5 to 12, while all other parameters were kept constant. According to the results obtained, the use of geogrids decreases vertical strains near the surface of the subgrade and leads to a reduction in pavement structure thickness. Overall, it can be concluded that optimal geogrid placement positively affects load distribution and provides improved structural characteristics.

3. Results

Table III indicates that the installation of geogrid at the interface of the subgrade and subbase results in a decrease in vertical strain at the top of the subgrade, regardless of CBR value and traffic loading. In the case of weak subgrades (CBR 5–6), maximum benefit from geogrid reinforcement can be achieved (reduction up to 16–20%) under high traffic loading conditions (20–30 msa). For medium CBR values (7–9), the reduction is noticeable but comparatively lower (approximately 7–15%), increasing with an increase in traffic loading.

Table 3. Percentage vertical strain reduction at the top of subgrade layer when geogrid is placed at the subgrade-subbase interface.

CBR	5 msa	10 msa	20 msa	30 msa
5	12.33	13.46	16.17	19.52
10	7.16	7.16	3.65	11.48
15	7.17	7.17	3.62	7.21

3.1. **Optimum Position of Geogrid on Pavement.** A number of tests were conducted to evaluate the effect of positioning the geogrid at various depths within the granular layer (0%, 20%, 60%, 80%, and 100% of base thickness) using a 700 kN/m biaxial geogrid subjected to a constant traffic load of 10 msa and subgrade CBR ranging between 5 and 12.
It was found that positioning the geogrid at 100% of the base thickness (subgrade-subbase interface) consistently resulted in the minimum vertical strain at the top of the subgrade. This confirms the suitability of this location as the optimum reinforcement position, as shown in Table IV. Comparative studies between reinforced and unreinforced pavement layers also demonstrated that this positioning resulted in lower strain values. Therefore, this location was adopted for the design recommendations.

Table 4. Vertical compressive strain produced at the top of the subgrade for varying CBR values under a 10 msa traffic load.

CBR%	UR	0%	40%	80%	100%
5	0.48	0.32	0.37	0.37	0.37
10	0.42	0.37	0.33	0.32	0.32
12	0.40	0.35	0.31	0.30	0.30

3.2. **Thickness Reduction of Granular Layer.** Once the geogrid was installed at 100% base depth, the WMM and GSB layers were optimized using a trial-and-error method while maintaining the vertical strain within the permissible limits of the subgrade (Table V). In this process, thickness reductions were initially performed in steps of 20 mm, followed by refinement of 5–10 mm for CBR values ranging from 5–15% and traffic loading from 5–15 msa. The results indicate that the geogrid layer provides an effective approach for reducing the thickness of the granular layer.

TABLE 5. Reduction in granular layer thickness in mm after reinforcement.

CBR (%)	5 msa	10 msa	20 msa	30 msa
5	70	80	90	170
10	25	35	40	60
15	20	25	30	35

3.3. **Service Life Ratio.** The Service Life Ratio (SLR) is presented in Table VI and is mathematically defined as the ratio of vertical compressive strain at the top of the subgrade in an unreinforced pavement condition to that in a reinforced condition. The SLR represents the strain improvement factor achieved due to the presence of reinforcement without modifying the existing pavement thickness.

For a constant CBR value with increasing traffic loading, the SLR value also increases, indicating the improved effectiveness of geogrid reinforcement under higher loading conditions.

TABLE 6. SLR of flexible pavement for subgrades with varying CBR and msa when a single-layer geogrid is provided at 100% of base thickness compared with unreinforced pavement.

CBR (%)	5 msa	10 msa	20 msa	30 msa
5	1.15	1.16	1.24	1.22
10	1.08	1.08	1.06	1.15
15	1.08	1.08	1.04	1.08

3.4. **Design Catalogue.** A complete catalogue covering CBR values between 5% and 15% and traffic loading between 5 and 30 msa has been prepared. The catalogue provides a practical approach for the design of geogrid-reinforced pavements and serves as an alternative to traditional design approaches [16]. Specifically, for CBR values ranging from 5% to 10%, which represent the most common governing subgrade strength conditions encountered in practice, significant improvement in pavement performance, structural stability, load distribution, and reduction in deformation can be achieved through geogrid reinforcement (Figures 3–5). Although the developed catalogue provides a consistent basis for the design of geogrid-reinforced pavements, site-specific conditions should be considered during the design process. The presented design catalogue can be used as a dynamic and evolving tool for designing innovative and sustainable pavement structures. Furthermore, design catalogues for intermediate CBR values have also been developed to facilitate interpolation. Therefore, pavement performance and required layer thicknesses can be estimated for intermediate subgrade conditions.

The analysis of design catalogues, as illustrated in Figure 3-5, shows that the use of geogrid reinforcement always allows the decrease in total thickness of the pavement structure regardless of the analyzed CBR value and traffic loading from 5 to 30 msa. From the comparison of unreinforced and reinforced designs, it can be concluded that the geogrid serves as an additional stabilizing factor, allowing the design of thinner granular base and sub-base layers without reducing the structural safety of the pavement. Such reduction in material volume demonstrates the mechanical benefits of geogrid inclusion, particularly in terms of providing additional lateral restraint and improving load-spreading capability. This aspect can also be further explored and quantified numerically.

As observed from the quantitative results, the influence of geogrids on pavement design parameters is maximum under critical conditions, i.e., the weakest subgrade and highest traffic loading. For example, at CBR = 5% and 30 msa traffic loading, the total pavement thickness is reduced from 715 mm for the unreinforced section to 555 mm for the reinforced section, resulting in a 22.4% reduction in material consumption. For other conditions, the percentage reduction in thickness varies but shows a clear increasing trend with higher traffic loading. For instance, the reduction

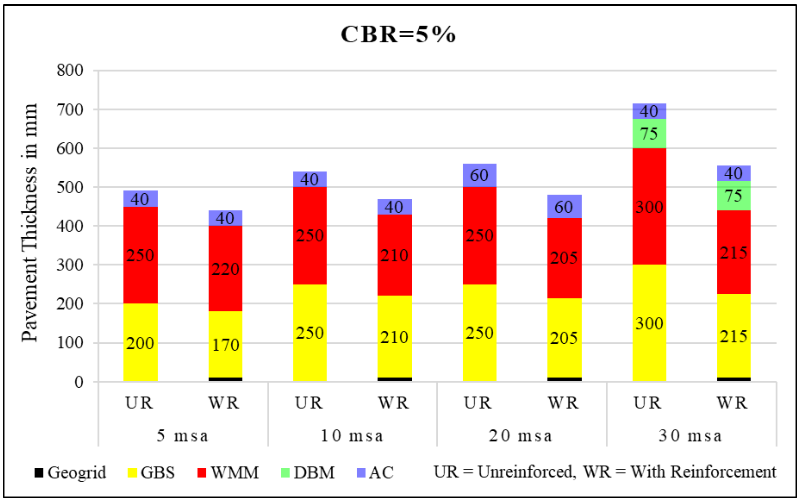

FIGURE 3. Catalogue for geogrid reinforced flexible pavement – CBR 5%.

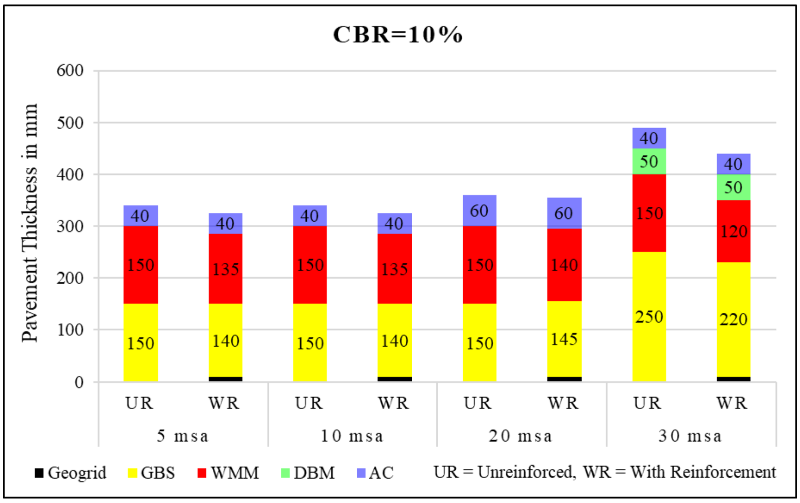

FIGURE 4. Catalogue for geogrid reinforced flexible pavement – CBR 10%.

is 10.2% for CBR = 10% and 30 msa, and 5.1% for CBR = 15% and 30 msa. These results demonstrate the potential of the developed tool as an engineering decision-support system.

3.5. **Validation of PLAXIS 3D Results with DoR Sheet and IIT Pave.** Validation of the PLAXIS 3D results with DoR Sheet and IIT Pave represents an important step toward demonstrating the reliability and accuracy of numerical modeling in pavement design. The surface and vertical deformation responses of the pavement model developed in PLAXIS 3D were evaluated using the same parameters adopted for manual calculations (Table VII and Figure 6).

According to the PLAXIS 3D results, the values of surface and vertical deformations were within the allowable limits specified by IIT Pave and FPDG (2021). Therefore, it can be concluded that PLAXIS 3D successfully represents the behavior of pavement structures under applied loading conditions. The capability of PLAXIS 3D to simulate physical pavement response makes it a valuable numerical tool for pavement design applications.

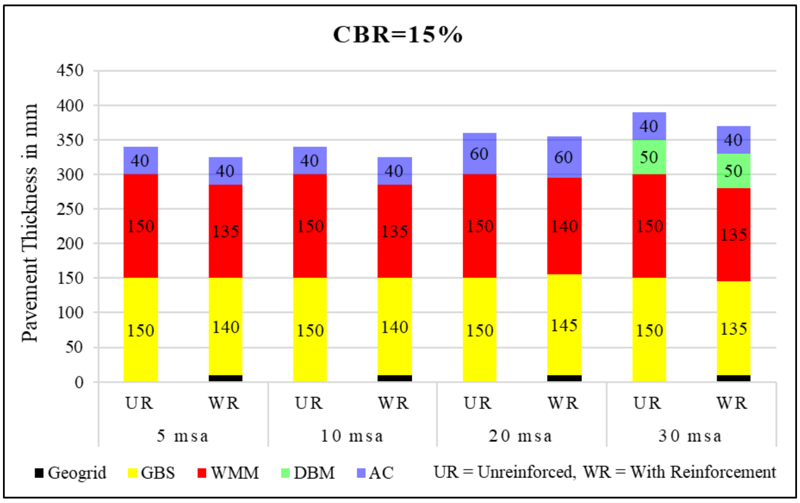

Figure 5. Catalogue for geogrid reinforced flexible pavement – CBR 15%.

The comparison of PLAXIS 3D predictions with DoR Sheet and IIT Pave results provides confidence in the accuracy and applicability of the numerical model. Based on these successful validations, the study was further extended toward developing design guidelines for geosynthetically stabilized road pavements.

Table 7. Vertical compressive strain at the top of subgrade obtained from PLAXIS 3D, DoR Sheet, and IIT-Pave.

Vertical Strain at Top of Subgrade with 30 msa Traffic Load						
CBR	5%	6%	7%	8%	9%	10%
PLAXIS	3.81E-04	3.63E-04	3.44E-04	3.23E-04	3.17E-04	3.15E-04
DoR Sheet	4.04E-04	4.08E-04	4.03E-04	3.76E-04	3.84E-04	3.98E-04
IIT Pave	3.35E-04	3.73E-04	3.93E-04	3.79E-04	4.13E-04	4.56E-04

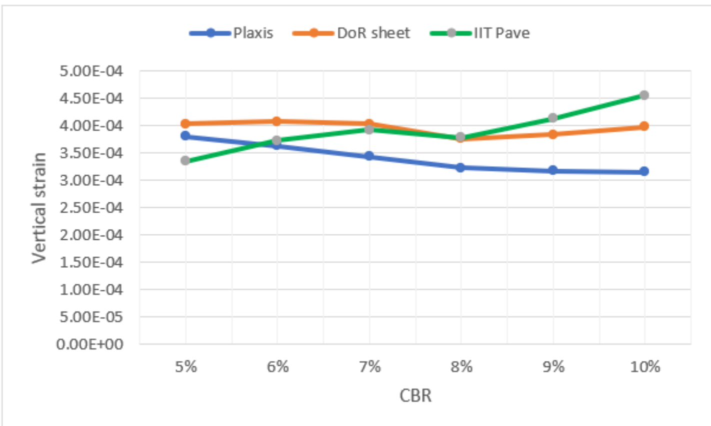

Figure 6. Comparison of vertical compressive strain at the top of subgrade.

The numerical model was also validated with field measurements from the Arughat–Okhale portion of the Mid-Hill Highway Project, Nepal [17]. The project site has been chosen near the Budhigandaki River Bridge, boarder of Gorkha and Dhading districts. Two pavement test sections have been used in the study. One was a non-reinforced pavement section at chainage (CH) 1+700 (28°2′22.51″N, 84°48′29.03″E), while another one was geogrid-reinforced pavement at chainage (CH) 1+800 (28°2′20.48″N, 84°48′27.42″E). The geogrid reinforcement was added to the Tensar 40/40Q geogrid at the mid-level of the pavement base. Earth pressure cells, strain gauges, and moisture sensors have been used at the geogrid level for monitoring of pavement response under dynamic traffic loading conditions.

Validation of the proposed design catalogue for the geogrids should take place by implementing it in the field and monitoring its performance over an extended period of time. Test pavement sections equipped with earth pressure cells, strain gauges, and moisture sensors can be created to monitor the pavement behavior under real traffic and environmental loads. Time series data should be acquired from the test sections and analyzed to assess the structural performance of the reinforced pavement and to validate the design guidelines proposed. Even though the repeated load analyses in PLAXIS 3D and the accelerated loading tests in the laboratory can be conducted as means of validation, the methods will be resource-intensive and costly.

4. Conclusion

These results clearly indicate that the use of geogrid reinforcement at the subgrade-subbase interface considerably decreases vertical compressive strain and allows large reductions in pavement thickness. With respect to subgrade CBR values of 5–15 and vehicle loads of 30 msa, the thickness of the base layer can be reduced by over 100 mm in weak subgrades (CBR 5–8) in case of loading of 30 msa, and by about 50–80 mm in case of loading of 20 msa, while keeping reasonable strains. From the above results, a catalogue of designs was proposed based on which, better structural efficiency, reduced construction costs, and a more environmentally-friendly pavement design were achieved. The numerical model was calibrated based on the geotechnical parameters determined from the Pulchowk Campus site, Lalitpur, Nepal; however, the calibrated numerical model provides a practical approach for numerical analysis as well as preliminary parametric studies at other sites, provided that appropriate adjustments are made in the input geotechnical parameters to consider the specific conditions of such sites. Since costs such as the initial cost, the cost of maintenance depending on rutting and fatigue, and the total cost of the project due to service life should be done separately from this paper, this limitation is also included within the scope of this research.

Acknowledgment. The authors gratefully acknowledge the support and facilities provided by the Research and Technology Unit (RTU), Pulchowk Campus, and the Quality Research and Development Center (QRDC), Department of Roads, Government of Nepal. Their assistance was invaluable in conducting this research. The author would like to acknowledge Er. Hemant Tiwari from SOTEN and Er. Vibek Gupta from SSTN for their supports and encouragements. Special appreciation is also given to Er. Sandeep Sapkota for his support during data logging under dynamic loading conditions of the vehicle and for providing essential logistical support throughout the field investigation.

References

[1] L. S. Calvarano, R. Palamara, G. Leonardi, and N. Moraci, "3d-fem analysis on geogrid reinforced flexible pavement roads," in *IOP Conference Series: Earth and Environmental Science*, vol. 95, 2017, p. 022024.

[2] J. Leng and M. A. Gabr, "Numerical analysis of stress–deformation response in reinforced unpaved road sections," *Geosynthetics International*, vol. 12, pp. 111–119, 2005.

[3] S. Perkins, "Mechanistic-empirical modeling and design model development of geosynthetic reinforced flexible pavements," Federal Highway Administration, Washington, DC, USA, Tech. Rep., 2001.

[4] S. Perkins and M. A. Ismeik, "A synthesis and evaluation of geosynthetic-reinforced base layers in flexible pavements – part ii," *Geosynthetics International*, vol. 4, pp. 605–621, 1997.

[5] M. Nazzal, M. Abu-Farsakh, and L. Mohammad, "Numerical analyses of geogrid reinforcement of flexible pavements," in *GeoCongress 2006: Geotechnical Engineering in the Information Technology Age.* Reston, VA, USA: ASCE, 2006, pp. 1–6.

[6] L. A. Al-Khateeb, A. Saoud, and M. F. Al-Msouti, “Rutting prediction of flexible pavements using finite element modeling,” *Jordan Journal of Civil Engineering*, vol. 5, pp. 173–190, 2011.

[7] L.-S. Gao, H.-C. Dan, and L. Li, “Response analysis of asphalt pavement under dynamic loadings: Loading equivalence,” *Mathematical Problems in Engineering*, vol. 2019, pp. 1–15, 2019.

[8] B. Saad, H. Mitri, and H. Poorooshasb, “Three-dimensional dynamic analysis of flexible conventional pavement foundation,” *Journal of Transportation Engineering*, vol. 131, pp. 460–469, 2005.

[9] B. Indraratna, N. T. Ngo, and C. Rujikiatkamjorn, “Behavior of geogrid-reinforced ballast under various levels of fouling,” *Geotextiles and Geomembranes*, vol. 29, no. 3, pp. 313–322, 2011.

[10] M. Y. Abu-Farsakh, J. Gu, G. Z. Voyiadjis, and Q. Chen, “Mechanistic–empirical analysis of the results of finite element analysis on flexible pavement with geogrid base reinforcement,” *International Journal of Pavement Engineering*, vol. 15, no. 9, pp. 786–798, 2014.

[11] M. Abu-Farsakh and Q. Chen, “Evaluation of geogrid base reinforcement in flexible pavement using cyclic plate load testing,” *International Journal of Pavement Engineering*, vol. 12, no. 3, pp. 275–288, 2011.

[12] S. K. Ahirwar and J. N. Mandal, “Finite element analysis of flexible pavement with geogrids,” *Procedia Engineering*, vol. 189, pp. 411–416, 2017.

[13] R. J. Bathurst and F. M. Naftchali, “Geosynthetic reinforcement stiffness for analytical and numerical modelling of reinforced soil structures,” *Geotextiles and Geomembranes*, vol. 49, no. 4, pp. 921–940, 2021.

[14] Federal Highway Administration, “Geosynthetic design and construction guidelines,” Federal Highway Administration, Tech. Rep., 2015.

[15] Indian Roads Congress, “Guidelines for the design of flexible pavements: Irc:37-2018 (4th revision),” Indian Roads Congress, Tech. Rep., 2018.

[16] Department of Roads, Ministry of Physical Infrastructure and Transport, “Flexible pavement design guidelines,” Government of Nepal, Kathmandu, Nepal, Tech. Rep., 2021.

[17] A. Tiwari, P. B. Shahi, R. Suwal, R. C. Tiwari, and P. K. Jha, “Evaluating geogrid-reinforced pavements with field-validated soil models under vehicle load dynamics,” *Journal on Transportation System and Engineering Research*, vol. 1, no. 2, pp. 37–49, 2025.